

1 **Origin and palaeo-environmental significance of the Berrazales carbonate spring**
2 **deposit, North of Gran Canaria Island, Spain**

3 Jon Camuera ^a, Ana M. Alonso-Zarza ^{a,b}, Álvaro Rodríguez-Berriguete ^{a,b}, Alejandro
4 Rodríguez-González ^c

5 ^a Dpto. Petrología y Geoquímica, Facultad de Ciencias Geológicas. Universidad
6 Complutense de Madrid. José Antonio Novais 12, 28040 Madrid, Spain

7 ^b Instituto de Geociencias (CSIC, UCM), José Antonio Nováis 12, 28040 Madrid, Spain

8 ^c Dpto. Física GEOVOL, Campus de Tafira, Universidad de Las Palmas de Gran
9 Canaria, 35017 Las Palmas de Gran Canaria, Spain

10 * Corresponding Author's telephone number and email: 913944915 /
11 jcamuera@gmail.com

12

13 **ABSTRACT**

14 The Berrazales carbonate spring deposit is a small outcrop constituted mainly by
15 cascade-like geometries. Four main facies have been identified: *Fibrous dense*
16 *macrocrystalline* formed by rapid degassing under high-flow conditions; *Framestones*
17 of coated plant molds formed in moderate energy flow favoured by the presence of
18 biogenic support; *Micrite/Microsparite* are primary precipitates in which crystalline
19 aggregates nucleated on organic filaments and/or EPS; *Banded micrite-coarse*
20 *crystalline* were the result of alternating physical-chemically and biologically induced
21 precipitation in areas of varying flow-velocities. Most facies underwent different
22 degrees of micritization processes. Micrite is distributed as thin lines penetrating the
23 crystals, as irregular patches or as micrite layers. In the first case organic filaments
24 penetrate crystals, suggesting that micritization is mainly biogenically driven. In the
25 latter cases micritization is caused mostly by partial dissolution. Microbe participation in

26 micrite formation increased micrite MgCO₃ content in comparison with coarse
27 crystalline facies.

28 Isotopic analyses show positive δ¹³C values (+2.63 and +4.29‰ VPDB) and negative
29 δ¹⁸O (-5.65 and -4.48‰ VPDB) values. Positive δ¹³C values clearly indicate fluids of
30 thermal volcanogenic origin.

31 The Berrazales spring deposit studied here very probably is a small part of a larger
32 carbonate building that was largely eroded by fluvial incision. Calculations of spring
33 water temperature give a range from 20°C to 35°C, characteristic of a cold to warm
34 spring favouring precipitation of calcite and important biogenic activity (*framestones*).
35 Although the study deposit has textural characteristics of tufas, provide that the CO₂
36 sourced from deep fluids, it should be consider as thermogene travertine, being one
37 more example of the difficulty of using those terms for ancient sedimentary deposits.
38 Carbonate springs deposits, very rare in the Canary Islands, are good archives of
39 recent volcanic activity, fluvial processes and vegetation regimes prevailing in the
40 islands in recent times.

41 *Keywords:* carbonate spring deposit; travertine facies; Canary Islands; microbes; stable
42 isotopes; volcanic setting.

43

44 **1. Introduction**

45 Calcareous spring deposits have been reported in various volcanic settings, such as in
46 the hot-spot of Yellowstone (Fouke, 2011), in the Bogoria and Turkana lakes of the
47 African Rift (Jones and Renaut, 1996; Renaut and Jones, 1997) and in arc-islands or
48 compressive systems as in Japan (Nishiwaka et al., 2012). Other calcareous spring
49 deposits are located along extensional fractures, such as the well-known Pamukkale-
50 Karahayit travertines in Turkey (Hancock et al., 1999; Özkul, 2005), the Tivoli area
51 (Gandin and Capezzuoli, 2014) or the Euganean geothermal field (Pola et al., 2014) in

52 Italy. The large hydrocarbon reservoir of the South-Atlantic Pre-salt also contains facies
53 similar to carbonate spring deposits (Terra et al., 2010). In spite of increasing interest in
54 the study of these deposits there is not yet a consensus on how to interpret many of
55 their facies, nor on the role of biogenic versus abiogenic processes in their formation or
56 on their classification (Ford and Pedley, 1996; Pentecost, 2005; Gandin and
57 Capezzuoli, 2008; Gandin and Capezzuoli, 2014). Lack of consensus continues
58 regarding calcareous spring deposits and also fluvial carbonates with regard to the use
59 of terms travertine and tufa. Originally, travertine has been applied to compact rocks
60 used for building construction material, whereas tufa usually denotes a softer more
61 friable deposit (Viles and Pentecost, 2008). Even so, recently these terms have been
62 scientifically redefined by some authors as Capezzuoli et al., (2014). Thus, travertine is
63 defined for non-marine carbonates formed from hydrothermal-sourced waters,
64 associated with tectonically active areas (and high geothermal heat flux) and
65 characterized mainly by high depositional rates, low porosity, regular bedding and fine
66 laminations, and an inorganic crystalline fabric. In contrast, the tufa is generally
67 produced from meteoric water at ambient temperature and characterized by low
68 depositional rates, high porosity and high content of microphytes and macrophytes
69 (Capezzuoli et al., 2014, Table 1). Temperature of water feeding the spring is other
70 classification criteria, although in cases it is difficult to apply to ancient deposits. Two
71 main types of waters may feed springs: 1) organic CO₂-rich and low temperature
72 waters (generally lower than 20°C) coming from the soil and groundwater form
73 meteogene travertines, which have negative $\delta^{13}\text{C}$ (-12 to -2‰ PDB) values; 2) $\delta^{13}\text{C}$
74 values of thermogene travertines, sourced from hot to warm waters (generally higher
75 than 30°C) coming from the interaction between host rock and CO₂ rich fluids at depth,
76 vary between -2 to +10‰ PDB (Kele et al., 2011; Capezzuoli et al., 2014). Mineralogy,
77 facies and microfacies of calcareous spring deposits are controlled by a set of
78 environmental parameters such as: water chemical composition and temperature, rate
79 CO₂ degassing, saturation levels and calcite deposition rate, macro and microbial

80 activity or the presence of some inhibitors (Talbot, 1990; Jones and Renaut, 2010; Guo
81 and Chafetz, 2014; Sun et al., 2014). This makes spring deposits good palaeo-
82 environmental archives (Andrews, 2006; Anzalone et al., 2007; Keppel et al., 2012;
83 Gradziński et al., 2013; Gradziński et al., 2014).

84 In the Canary Islands carbonate spring deposits are very scarce (Demény et al., 2010,
85 Alonso-Zarza et al., 2012; Rodríguez-Berriguete, 2012). In this paper we study the
86 Berrazales spring deposit, located in Gran Canaria Island. Our aims are to unravel: a)
87 the thermal-volcanic influence in the formation of carbonate spring deposits in volcanic
88 settings, b) the role of biogenic versus abiogenic processes and their interrelation
89 during and after crystalline growth and, c) water physicochemical conditions
90 (temperature, pH, chemistry, etc.) controlling the formation of the deposits. Our
91 conclusions can be an aid to the understanding of the processes and the main controls
92 involved in the formation of travertines in volcanic settings and their palaeo-
93 environmental and palaeo-hydrological significance.

94

95 **2. Geographical and geological setting**

96 The Canary Islands (Spain) are located off the NW African coast, between 29° 25' and
97 27° 37' N and 18° 10' and 13° 20' W, developed over the Jurassic oceanic lithosphere
98 as a result of the eastward movement of the African plate over a mantle hotspot (Holik
99 et al., 1991; Carracedo et al., 1998; Carracedo et al., 2002). Similar to other intra-plate
100 volcanic islands, the Canarian archipelago displays the hotspot volcanic stages of
101 evolution: juvenile (shield), volcanic quiescence and rejuvenated stage. Gran Canaria,
102 actually in an advanced rejuvenated stage, is a nearly circular island located at the
103 centre of the Canarian archipelago. A dense radial network of deep ravines
104 ("barrancos", the local toponymy) dissects the island, forming a rugged topography.
105 The sub-aerial development of Gran Canaria records a juvenile stage (ca. 14.5–8.0
106 Ma), a volcanic quiescent stage (ca. 8.0–5.5 Ma) and a rejuvenated stage (ca. 5.5 Ma

107 to present) including the Roque Nublo stratovolcano and the Post-Roque Nublo
108 volcanism (Pérez-Torrado et al., 1995; Carracedo et al., 2002; Guillou et al., 2004;
109 Aulinas et al., 2010). The most recent Post-Roque Nublo volcanism, Holocene in age,
110 created a monogenetic volcanic field with at least 24 vents. The eruptive style is mainly
111 strombolian with formation of small scoria cones and lava flows, mostly with aá
112 morphologies (Rodríguez-González et al., 2009; Rodríguez-González et al., 2012). The
113 Holocene vulcanism has a strong control on the development of the few carbonate
114 spring deposits have been studied in Gran Canaria. One of these deposit is Azuaje
115 travertine described by Rodríguez-Berriguete et al. (2012) located 9 km north-east of
116 the study area.

117 The carbonate deposits studied are located above the stratigraphic contact between
118 scoria cone and lava flow of the Berrazales eruption (Fig. 1A), in the upper part of
119 Barranco Los Ríos (Fig. 1B). The lava flow is classified as basanite (Rodríguez-
120 González et al., 2009). Holocene lava flows were emplaced at the bottom of the
121 ravines, with little erosive incision and draining towards the coast (Rodríguez-González
122 et al., 2009; Rodríguez-González et al., 2012). This eruption is stratigraphically related
123 with Jabalobos (dated by ^{14}C at $2,760 \pm 60$ BP) and Fagajesto (dated by ^{14}C at $3,030 \pm$
124 90 BP) eruptions (Rodríguez-González et al., 2009; Aulinas et al., 2010).

125

126 **3. Methods**

127 Samples of the Berrazales outcrop were studied using conventional petrological,
128 mineralogical and geochemical analyses. Twenty six samples were chosen for
129 conventional optical petrographic study in thin sections. Fragile thin sections were
130 impregnated with epoxy resin.

131 Mineralogical semi-quantitative composition of all samples was determined by X-ray
132 powder diffraction (XRD) using a Philips PW-1710 with $\text{CuK}\alpha$ at 40 KV and 30 mA.

133 MgCO₃ mole percent is measured from d-spacing of calcite crystal lattice, which was
134 determined by the variation of 2 θ value of the principal calcite peak of the X-ray
135 diffractograms (Goldsmith et al., 1961; Tucker, 1988; Scholle and Ulmer-Scholle, 2003;
136 Ries et al., 2008).

137 The texture and components studied in 12 gold-coated samples were determined using
138 a JEOL JSM 6400 scanning electron microscope on the Research Support Centre
139 (CAI) of Geological Techniques of UCM (Madrid, Spain), working at 20kV with a
140 resolution of 35Å. Secondary electron and backscattering detectors were used together
141 with an X-ray detector system to obtain semi-quantitative compositions. For the study it
142 was also necessary to use a FEI INSPECT (5350 NE Dawson Creek Drive Hillsboro,
143 Oregon 97124, USA) of the Museo Nacional de Ciencias Naturales (Madrid, Spain),
144 operating with high vacuum mode (0.08 to 0.60 torr) with conductive samples to be
145 studied with both the large field detector (LFD) and backscatter detector (BSED-
146 detector electron backscatter). SEM resolution at high vacuum was 3.0 nm at 30 kV
147 (SE), 10 nm at 3 kV (SE), and 4.0 nm at 30 kV (BSE). The accelerating voltage was
148 20-30 kV, high vacuum 0.45 torr, working distance of 10 mm.

149 The $\delta^{13}\text{C}$ and $\delta^{18}\text{O}$ values from 21 selected powdered samples were analysed at the
150 Scientific and Technical Survey in Barcelona University (Spain). Samples were
151 obtained with a drill and reacted with 100% phosphoric acid at 70°C for 3 minutes. CO₂
152 was extracted using a Thermo Finnigan Carbonate Kiel Device III isotopic analyzer with
153 a Thermo Finnigan MAT-252 spectrometer, according to the McCrea (1950) method.
154 $\delta^{13}\text{C}$ and $\delta^{18}\text{O}$ values, corrected using the NBS-19 standard and with an analytical
155 precision of $\pm 0.02\text{‰}$ for $\delta^{13}\text{C}$ and 0.03‰ for $\delta^{18}\text{O}$, are expressed in parts per thousand
156 (‰) referred to VPDB standard.

157

158 **4. Results**

159 *4.1. Outcrop features of the Berrazales carbonate deposit*

160 Berrazales carbonate deposit is a small outcrop approximately 6-7 m long, located
161 between volcanic cinder cones and Holocene lava materials. The outcrop has three
162 sectors: the eastern sector consists of cascade morphologies dipping to the east; the
163 western sector dips to the west; in the central sector the cascades are vertical. In the
164 eastern side the cascade geometries include large molds of tree trunks, one with a
165 diameter larger than 50 cm.

166 Individual carbonate cascade bodies, of a maximum height of 3 m and width of about
167 0.5-1.5 m, are composed of various vertical to oblique irregular centimeter-thick beds
168 (Fig. 2A, B).

169

170 *4.2. Facies and microfacies: description and interpretation*

171

172 *4.2.1. Fibrous dense macrocrystalline facies*

173 *Description*

174 *Fibrous dense macrocrystalline facies*, 1.5-2.0 cm thick bands of fibrous pale calcite
175 crystals, 1.0-1.5 cm long and length-width ratio >10:1 (Fig. 3A) have intercalations of
176 micritic and more porous laminae. Fibrous crystals nucleate and grow on sub-
177 horizontal surfaces or on plant molds and have branching feather or dendrite
178 morphologies (Jones and Kahle, 1986; Jones and Kahle, 1993; Guo and Riding, 1992;
179 Jones et al., 2000; Kele et al., 2011). Sometimes feather or dendritic crystals appear
180 growing from a small filament (>300 µm long and around 12 µm thick) (Janssen et al.,
181 1999; Gradziński, 2010) (Fig. 3B). Thin light-brown laminae (2-15 µm thick) are
182 included within the feather crystals. Also brownish-black darker laminae (10-15 µm
183 thick) separate dendritic crystalline bands (Fig. 3A). Above those laminae there are

184 small inclusions of triangular microsparite crystals inside large fibrous crystals (Freytet
185 and Verrecchia, 1999). Both light-brown and brownish-black sheets are curved and
186 acquire the upper surface morphology of dendrites. Terminations of fibrous crystals are
187 micritized (Fig. 3C, D) by microbes. Microbial filaments also penetrate coarse crystals
188 generating microborings (Fig. 3D, E) and parallel tubular porosity (Fig. 3F).

189

190 *Interpretation*

191 These crystalline facies appear to be the product of rapid precipitation from
192 supersaturated water with respect to calcite due to rapid CO₂ degassing under
193 disequilibrium conditions (Jones et al., 2005). In particular, calcite branching feathers or
194 dendrites have been described in areas of rapid growth (Jones and Kahle, 1986) due to
195 high-flow conditions (~2 m/s) (Okumura et al., 2012) favouring rapid CO₂ loss. Thin
196 light-brown laminae alternating within feathers are the result of temporal variations in
197 precipitation, probably caused by rhythmic increases-decreases in diverse atomic
198 element content, such as Fe, probably reflecting recurrent annual growth cycles (Jones
199 et al., 2005; Jones and Renaut, 2008). Brownish-black laminae indicate stages of
200 interrupted crystal feather growth, due to variations in water geochemistry (presence of
201 undersaturated waters, low flow rates, microbial activity, etc.). Even so, the presence of
202 organic matter as the origin for brownish-black laminae cannot be ruled out, as
203 described by Freytet and Verrecchia (1999). Connected circular microborings are due
204 to the activity of microbes, such as cyanobacteria (Radtke and Golubic, 2011; Okumura
205 et al., 2012) or fungi (Calvet, 1982; Golubic et al., 2005) which penetrate, dissolve and
206 micritize calcite crystals.

207

208 *4.2.2. Framestone facies*

209 *Description*

210 *Framestone* is a porous macrocrystalline facies mostly composed of subparallel coated
211 plant molds 1-3 cm long and 0.5-8 mm in diameter (Fig. 4A). As in *fibrous dense*
212 *macrocrystalline* facies, small fibrous crystals (<3 mm long) are arranged perpendicular
213 to molds, forming fans (~3 mm) and including thin light-brown lamination (2-15 μ m
214 thick) (Fig. 4B). The top surfaces of fans are covered by a dark-brown irregular micritic
215 mass (<0.2 mm thick). Micrite is also distributed between large fibrous crystals. Note
216 that plants molds have also well-defined parallel structure (Fig. 4C).

217

218 *Interpretation*

219 Vegetal molds provided nuclei for the precipitation of crystalline fans. Similar but larger
220 fans described on Pancura Pitu's travertine (Centra Java, Indonesia) by Okumura et al.
221 (2012) were interpreted as having been precipitated under fast-flow conditions (~2
222 m/s). In our case flow velocities were probably lower than 2 m/s, as indicated by the
223 smaller size of fans and by the presence of plant molds, whose preservation would
224 have been inhibited under very high energy water (Okumura et al., 2012). Dark-brown
225 micritic masses are formed by the breakdown of coarse calcite crystals by abiogenic or
226 biogenic processes (Kobluk and Risk, 1977; Calvet, 1982; Jones and Kahle, 1995;
227 Martín-García et al., 2009). Even so, lack of biogenic features, such as filaments or
228 cyanobacterial microborings, suggest that dark micrite masses were formed by
229 abiogenic processes.

230

231 *4.2.3. Micrite-coarse banded crystalline facies*

232 *Description*

233 *Micrite-coarse banded crystalline* facies consist of palisade calcite crystals (up to 1 mm
234 long) sub-perpendicular to substrate. Crystals include very thin (2-10 μ m) reddish-
235 translucent microlaminae and dark-micritic laminae (Fig. 4D). Reddish-translucent

236 microlaminae are laterally very uniform and regular whereas dark-micritic ones are
237 more irregular. V-shaped morphologies of both laminae are governed by the
238 morphology of crystal edges. Sometimes the laminae penetrate crystal edges. Dark
239 micritic laminae are amalgamated and contain very small filaments (<0.1 mm long) in
240 contact with the external surface.

241

242 *Interpretation*

243 The lack of any biogenic features in the palisadic crystals suggests that purely
244 physicochemical processes mainly governed crystal formation (Riding, 2008). The thin
245 reddish translucent microlaminae are similar to those described in the afore-mentioned
246 *fibrous dense macrocrystalline* facies, indicating cyclic changes in chemical, physical
247 and/or environmental conditions (Valero-Garcés et al., 2001) or even diurnal cycles of
248 microbial activities (Okumura et al., 2013a; Okumura et al., 2013b). Dark micritic
249 laminae within the palisade crystals are probably formed when calcite crystals come
250 into contact with undersaturated fluids with respect to CaCO₃ (Jones and Kahle, 1995)
251 as also described in coarse crystalline speleothems (Martín-García et al., 2009), or due
252 to the presence of very small concentrations of organic matter (Pedley, 1992;
253 Gradziński, 2010). Small filaments on external surfaces suggest that biological
254 micritization of those dark-micritic laminae cannot be ruled out.

255

256 *4.2.4. Micrite/Microsparitic facies*

257 *Description*

258 *Micrite* (<4 µm) / *Microsparitic* (4-100 µm) facies are either homogeneous or banded.
259 Homogeneous microfacies are composed of micrite/microsparitic masses which
260 include crystalline aggregates of pale calcite crystals, arranged on thin organic
261 filaments (~700 µm long and <10 µm thick). Transversally, these aggregates have

262 spherulitic morphologies (Fig. 5A). Banded microfacies consist of an alternation of: a)
263 Microsparitic bands containing crystalline fans (~500 µm) (Fig. 5B); b) Dendrolitic fabric
264 (Perri et al., 2012) composed of filamentous cyanobacteria (500-800 µm long) arranged
265 vertically and calcified by sparite crystals (around 100-200 µm long) (Fig. 5C, D) with a
266 length-width ratio of 3:1; c) Dark micritic layers around 0.2 mm thick; d) Irregular porous
267 sheets (>0.5 mm thick) with semi-circular pores (0.5 mm to 1.5 cm across), making the
268 rock significantly porous. Some pores are filled by light-translucent bladed sparitic
269 crystals (around 100 µm long and 25 µm thick) arranged as gravitational, meniscus and
270 also as isopachous cements. These facies also contain not-mineralized exopolymeric
271 substances (EPS) (Fig. 5E, F) from microbial activity.

272

273 *Interpretation*

274 Lack of dissolution features of crystalline aggregates and absence of any primary fabric
275 substitution suggest that micrite/microsparite is a primary precipitate. Crystalline
276 aggregates probably nucleated on organic filaments which provided a site for calcium
277 carbonate nucleation (Pentecost, 2005). Several studies have linked the formation of
278 similar spherulites with microbial activity, which generated a favourable
279 microenvironment for Ca²⁺ and Mg²⁺ concentration and calcium carbonate precipitation
280 (Castanier et al., 1989; Buczynski and Chafetz, 1991). Similar processes led to both
281 the formation of crystalline fans, as the result of initial calcite nucleation on biogenic
282 structures within the micrite, and subsequent growth by purely physicochemical
283 processes (CO₂ degassing, evaporation...) (Jones and Renaut, 2010). However,
284 organic nuclei are not always preserved (Guo and Riding, 1992), because bacteria and
285 cyanobacteria may be completely destroyed within hours by crystal growth (Krumbein
286 et al., 1977).

287 Dark micritic layers probably represent the precipitation of micrite on extracellular
288 polymeric substances (EPS) (Chacón et al., 2006) in association with cyanobacteria

289 and biological processes (Perri et al., 2012). EPS can be partially decomposed by
290 aerobic heterotrophic bacteria, inducing CaCO₃ precipitation (Dupraz et al., 2004;
291 Gautret et al., 2004; Decho et al., 2005). The result is the calcification of the EPS
292 biofilm by micritic crystals (Turner and Jones, 2005; Okumura et al., 2013b).

293 Irregular porous sheets may result from dissolution of micrite precipitated on EPS or
294 from organic matter degradation (Perri et al., 2012). Gravitational and meniscus
295 cements consist of bladed crystals, suggesting that samples were subject to both
296 vadose and phreatic post-depositional processes.

297

298 *4.3. Diagenetic features*

299 The main diagenetic processes that influence the final aspect of Berrazales travertine
300 are micritization, dissolution and cementation.

301 Micritization consists of partial or total substitution of coarse calcite crystals by a mass
302 of micritic/microsparitic calcite crystals (2-15 µm). There are two types of micritization.
303 The first type affected some specific bands and the topmost fibrous feather crystals of
304 *fibrous dense macrocrystalline* facies. Bands less than 1 cm thick are composed of
305 irregular micrite patches alternating with non-micritized fibrous calcite crystals (Fig. 6A).
306 Besides, tops of fibrous feather and dendrite crystals are also perforated by a biogenic
307 network (Fig. 6B) composed of thin microbial filaments (Fig. 6C), suggesting a biogenic
308 origin for micritization (Radtke and Golubic, 2011; Okumura et al., 2012). Microspar is
309 considered an intermediate product between coarse calcite and micrite.

310 The second type of micritization consists of thin micritic laminae (2-15 µm) separating
311 large crystal formations, mainly in *micrite-coarse banded crystalline* facies and in
312 *fibrous dense macrocrystalline* facies. Lack of biogenic features in *framestone* facies
313 and the fact that micrite does not penetrate in large crystals suggests that micrite
314 formation is due to inorganic physicochemical changes, probably caused by

315 undersaturated water inflow or variations in environmental conditions (Jones and Kahle,
316 1995; Martín-García et al., 2009).

317 Dissolution processes also play an important role in micritic/microsparitic samples,
318 forming irregular and non-continuous, fenestral-like porosities. Dissolution may be due
319 to undersaturated calcite water input (Martín-García et al., 2009) and/or due to the
320 degradation of microbial organic matter.

321 Cements occur in *micrite/microsparitic* facies either as bladed calcite crystals (80-150
322 μm long) covering the whole surface of the pore or as meniscus and gravitational
323 cements, indicating that cementation occurred in both vadose and phreatic
324 environments.

325

326 *4.4. Mineralogy and isotope geochemistry*

327 Samples are mainly (proportions higher than 95%) composed of Low Magnesium
328 Calcite (LMC) along with minor traces of phyllosilicates (< 5%). Content of MgCO_3 in
329 most samples varies between 2% and 5%, except in sample BER-17 which has two
330 calcite peaks corresponding to two calcite phases with 4% and 11% in moles of MgCO_3
331 (Table 1). In general, higher Mg contents (4-11% in moles of MgCO_3) are in
332 *micrite/microsparitic* facies. Macrocrystalline facies (*fibrous dense macrocrystalline*
333 facies and *framestone* facies) contain between 0% and 3% in moles of MgCO_3
334 whereas *micrite-coarse banded crystalline* facies lack magnesium (Table 1).

335 Isotopic values obtained from different facies show only slight variations in $\delta^{13}\text{C}$ and in
336 $\delta^{18}\text{O}$, probably due to the small size of the outcrop and absence of fractionation
337 between water and mineral phase (HCO_3^-). All samples have positive (+2.63 and
338 +4.29‰ VPDB) $\delta^{13}\text{C}$ and negative (-5.65 and -4.48‰ VPDB) $\delta^{18}\text{O}$ values (Fig. 7A, B),
339 with a correlation coefficient of 0.59. The lightest values of $\delta^{18}\text{O}$ correspond to the
340 macrocrystalline samples while heaviest ones are found in micritic facies, which are

341 also enriched in Mg. Some micritized bands in macrocrystalline facies show an
342 increase in $\delta^{18}\text{O}$ relative to non-micritized ones. Changes between different facies in
343 $\delta^{13}\text{C}$ show smaller variations.

344

345 **5. Discussion**

346 *5.1. Facies types, biogenic versus abiogenic processes and palaeo-environmental* 347 *setting*

348 The small Berrazales deposit, one of the few carbonate deposits found in Gran Canaria
349 Island, outcrops in Los Rios Valley, formed after the last volcanic event around 2,700 –
350 3,100 years ago, surely in relation with volcanic eruptions occurred in Jabalobos and
351 Fagajesto (Fig. 1A). Its exceptional situation on a recent lava flow deposit, along with
352 its cascade morphology, strongly suggests formation from spring waters, similar to
353 nearby Azuaje travertine (Rodríguez-Berriguete et al., 2012).

354 Facies indicate different conditions for calcite precipitation. *Fibrous dense*
355 *macrocrystalline* facies precipitated during rapid CO_2 degassing (Jones et al., 2005),
356 favouring the rapid growth of fibrous branching feather or dendrite crystals (Jones and
357 Kahle, 1986; Okumura et al., 2012). Vegetal molds, stems and microbial filaments act
358 as support and nuclei for calcite precipitation. In *framestone* facies, the absence of
359 reworking and preservation of molds in live position suggest that water-flow velocity
360 was not higher than <2 m/s (Okumura et al., 2012), allowing growth and later
361 calcification of vegetal molds. In contrast, primary micrite precipitated in a calm water
362 environment highly saturated in CaCO_3 (Jones and Kahle, 1995).

363 It is difficult in these deposits to distinguish the role of biogenic from abiogenic
364 processes in the formation of the various facies. In most cases both processes acted
365 together. For example, the formation of fibrous feather crystals faithfully reflects the
366 interaction of biogenic and abiogenic processes and denote changing of crystallization

367 rates of calcite. In a first stage, microbial filaments (Fig. 8A) act as templates for small
368 calcite crystal (up to 100 μm long) nucleation (Fig. 3B; Fig. 5A, C, D; Fig. 8B). Organic
369 filaments provided a favourable site for calcite nucleation (Pentecost, 2005; Gradziński,
370 2010) and a good microenvironment for Ca^{2+} and Mg^{2+} concentration (Castanier et al.,
371 1989; Buczynski and Chafetz, 1991), although the slow crystal growth allows filaments
372 not to be completely entombed. In contrast, during a second stage, crystallization rate
373 is too fast for microbial community and physicochemical precipitation prevails. Thus,
374 the rapid growth of calcite, principally due to the rapid abiogenic CO_2 degassing,
375 enables the development of large branching feathers or dendrites (Fig. 3A; Fig. 8C). In
376 a final stage, large fibrous crystals are infected by microbes (fungi or cyanobacteria)
377 (Fig. 3E and Fig. 6C), which penetrate them causing partial micritization (Fig. 3C, D;
378 Fig. 6A, B; Fig. 8D) (Radtke and Golubic, 2011; Okumura et al., 2012). These microbial
379 colonization indicate a diminishing growth rate of crystals or their completely cessation.
380 On the contrary, *framestone* facies underwent abiogenic micritization by dissolution
381 caused by undersaturated water inflow (Fig. 4B) (Jones and Kahle, 1995; Martín-García
382 et al., 2009).

383 A more clearly biogenic influence is seen in the formation of micrite/microsparite with
384 higher MgCO_3 due to the replacement of exopolymeric substances (EPS) by high
385 magnesium calcite (HMC) (Dupraz et al., 2004; Dupraz and Visscher, 2005). The
386 degradation of EPS by heterotrophic bacteria (Decho et al, 2005) liberates Ca^{+2} , Mg^{+2}
387 and HCO_3^- which were bound to EPS, increasing cation concentration in solution and
388 allowing micritic Mg-calcite precipitation (Dupraz et al., 2004, Okumura et al., 2013a).

389

390 5.2 Discussion of stable isotope data

391 The $\delta^{13}\text{C}$ and $\delta^{18}\text{O}$ values in continental carbonate deposits are mainly controlled by
392 the isotopic composition of water, temperature of formation, pH of the solution, calcite
393 deposition rate, saturation degree, diagenesis, microbial activity, evaporation, CO_2

394 outgassing and fractionation between water and mineral phase (Talbot, 1990; Valero-
395 Garcés et al., 2001; Dietzel et al., 2009; Guo and Chafetz, 2014; Sun et al., 2014).

396 Positive $\delta^{13}\text{C}$ values indicate “deep-source” fluids in relation with volcanic activity or
397 decarbonation (Pentecost, 2005). Considering the volcanic area of the study, $\delta^{13}\text{C}$
398 positive values of Berrazales may suggest that this continental deposit was precipitated
399 from thermal waters which were saturated with heavy CO_2 from bedrock (Özkul et al.,
400 2014), influenced by significant contribution of volcanic-hydrothermal CO_2 . Carbonate
401 spring deposits precipitated from heavy hydrothermal CO_2 waters, have typical values
402 ranging between -2 and +10‰ PDB (Pentecost, 1995; Pentecost, 2005; Viles and
403 Pentecost, 2008). The Berrazales deposit is in this range, with similar $\delta^{13}\text{C}$ values to
404 the Azuaje travertine described by Rodríguez-Berriguete et al. (2012) and to other
405 travertines of the world (Fig. 9). These deposits can be classified as thermogene
406 deposits following Pentecost (2005) classification. $\delta^{13}\text{C}$ values in hot-water travertine
407 deposits are mainly controlled by physical (CO_2 degassing or water temperature) and
408 microbial processes (Kele et al., 2008; García-del-Cura et al., 2014). On the other
409 hand, changes in $\delta^{18}\text{O}$ values can also reflect the effect of evaporation, temperature of
410 water and, at the time of precipitation, degassing of CO_2 and/or groundwater inflow
411 (Chafetz and Lawrence, 1994; Valero-Garcés et al., 2001; Kele et al., 2008). In
412 Berrazales deposit changes in evaporation, water temperature or degassing were
413 probably not significant because the small size of the deposit did not allow water to re-
414 equilibrate. CO_2 removal and subsequent variations in $\delta^{13}\text{C}$ values in Berrazales
415 travertine could occur due to biological processes, such as respiration or microbial
416 photosynthesis (García-del-Cura et al., 2014). Microbes consumed preferably the
417 lighter carbon isotope, enriching water and the precipitated calcite in the heaviest
418 isotope, as shown by heavy $\delta^{13}\text{C}$ values and high Mg content on micrite/microsparite,
419 precipitated under the influence of EPS.

420 A temperature of 23°C of the water of the abandoned spa, placed 570 m downflow of
421 the Berrazales deposit (Garraalda-Iribarren, 1952) and the $\delta^{18}\text{O}$ values of the crystalline

422 crust (sample BER-11) were used to obtain the possible original $\delta^{18}\text{O}$ signal of the
423 water precipitating this crust. A value of -3.33‰ V-SMOW was obtained for equilibrium
424 precipitation using Kim and O'Neil (1997) equation, whereas the value for
425 disequilibrium conditions, obtained through Halas and Wolacewicz, (1982) equation,
426 according to Kele et al. (2011), was 5.5‰ V-SMOW. These values, which are in the
427 range of the reported from Gran Canaria Island, -2 to -6‰ , (Gonfiantini et al, 1976;
428 Gasparini et al., 1990), were used to calculate the probable temperature of precipitation
429 of the other facies of the deposit (Table 2A, B).

430 Temperatures obtained under equilibrium conditions and $\delta^{18}\text{O}_w = -5.5\text{‰}$ (9.4 to 14.8°C)
431 are very low compared to reported groundwater temperatures for Gran Canaria Island
432 of 14 - 35°C (Gonfiantini et al., 1976; Custodio et al., 1987; Gasparini et al., 1990). The
433 later are similar to temperature calculations under disequilibrium (19.7 - 35.4°C) and fit
434 well with the measured value of 23°C (Garralda-Iribarren, 1952). Cooling trends in
435 surface needed to pass from, at least, 23°C (at spring) to 9°C (downflow) are also
436 highly improbable at this altitude on Gran Canaria Island, suggesting that if calcite
437 precipitated from waters with $\delta^{18}\text{O}_w = -5.5\text{‰}$ (or slightly higher values) at about 23°C , it
438 occurred under disequilibrium conditions (Table 2B). The relatively narrow values of
439 temperatures obtained for the different facies indicate that the probable vent (crystalline
440 crust) and cascade deposits (the other facies) were very near as shown by the small
441 size of the Berrazales outcrop. However, these calculations may be not that precise as
442 desirable, as for example there may be ^{18}O isotope shift effects and temperature could
443 have changed along the life of the spring.

444 $\delta^{13}\text{C}$ value from the same sample has been used to obtain the original signal of $\delta^{13}\text{C}_{\text{CO}_2}$
445 (Table 3). The values obtained using Mook et al. (1974) $\text{HCO}_3^- - \text{CO}_2(\text{g})$ equilibrium
446 equation (used here for disequilibrium precipitation) are similar to those of fluids
447 derived from tectono-metamorphic processes (Hoefs, 1997; Minissale, 2004).
448 However, they are in the range of those reported in literature as volcanic originated
449 fluids from Canary Islands, which are usually higher than -4‰ (Albert et al., 1986;

450 Custodio et al., 1987; Gasparini et al., 1990). The calculated values using Bottinga
451 (1968) and Panichi and Tongiorgi (1976) equations (Table 3) fit well with the typical
452 range of volcanic CO₂, -5 to -7‰ PDB (Hoefs, 1997), which are slightly lighter than
453 those of the volcanic CO₂. Therefore, only deep source for CO₂ can be invoked here
454 through isotopic calculations, and no precisions between tectono-metamorphic derived
455 or volcanic derived CO₂ can be assessed. However, giving the overall setting, the CO₂
456 was probably of volcanic origin.

457

458 **6. Conclusions**

459 The Berrazales carbonate building is characterized mainly by cascade morphologies,
460 with different types of facies, such as (1) *Fibrous dense macrocrystalline facies*, (2)
461 *Framestone facies*, (3) *Micrite/microsparitic facies* and (4) *Micrite-coarse banded*
462 *crystalline facies*. Fibrous feather or dendrite crystals grew from the interaction
463 between biogenic and abiogenic processes, starting from crystalline nucleation on
464 microbial filaments to the last phase of rapid physicochemical crystal growth (CO₂
465 degassing) under rapid water flow and disequilibrium conditions. In *Framestone facies*,
466 presence of parallel plant molds suggests that water energy could not be very high (<2
467 m/s), preserving plants apparently in live positions. On the contrary, primary micrite
468 precipitated during lower flow and calmer waters probably in relation with EPS. Finally,
469 the thin banded facies indicate chemical, physical or environmental changes during
470 carbonate precipitation. Micritization processes are also under both biogenic (crystal
471 perforations by microbial filaments) and abiogenic (undersaturated water inflow, changes
472 in environmental conditions) processes.

473 Calcite is the principal mineral making up the travertine, generally with low Mg
474 contents, except micritic samples formed from microbial activities and EPS formation.

475 Positive $\delta^{13}\text{C}$ values (+2.63 and +4.29‰ VPDB) found in thermogene travertines
476 indicate formation from “deep source” fluids, in this volcanic area probably related with
477 thermal waters and volcanic activity. Whereas, negative $\delta^{18}\text{O}$ values (-5.65 and -4.48‰
478 VPDB) reflect a meteoric water signal. Thus, temperatures calculated (20-35°C), heavy
479 $\delta^{13}\text{C}$ values and the situation of the Berrazales deposit indicate that the CO_2 was very
480 probably of thermal origin and sourced from or below the Earth`s crust.

481 As are other thermogene spring deposits in Gran Canaria, Berrazales carbonate
482 deposit is an excellent example of the interplay between volcanic and sedimentary
483 processes, due to its location on previous volcanic materials deposited 2,700 – 3,100
484 years ago. The described deposit is a particular case study of a carbonate spring which
485 from the textural point of view can be classified as tufa (meteogene travertine) but from
486 the geochemical point of view ($\delta^{13}\text{C}$) as travertine (thermogene travertine).

487 The study of the Berrazales deposit has provided valuable information about thermal
488 water temperature, volcanic CO_2 contribution to thermal water springs, the role of
489 abiogenic versus biogenic processes in its formation and the presence of fresh water
490 streams in the island. At present very few examples of carbonate springs have been
491 described in the Canary Islands as their preservation in erosive regimes of volcanic
492 settings is exceptional.

493

494 **7. Acknowledgements**

495 We acknowledge A. Meléndez, M.C. Cabrera and J.F. Pérez-Torrado for his assistance
496 during the field work. James Cerne reviewed the English version of the manuscript.
497 Special thanks for Xabi Arroyo from CAI of Geological Techniques of UCM and to the
498 reviewers, Michal Gradziński and anonymous one, for their suggestions and
499 comments. This research was funded by Project CGL-2011-27826-CO2-01 from
500 MINECO.

501

502 **8. References**

503 Albert, J.F., Araña, V., Diez, J.L., Filly, A., Fontes, J.C., 1986. Modelo termodinámico
504 de la actividad del Teide. *Anales de Física, Series B: Aplicaciones, métodos e*
505 *instrumentos* 82, 86-201.

506 Alonso-Zarza, A.M., Rodríguez-Berriguete, A., Cabrera, M.C., Meléndez, A., Martín-
507 Rodríguez, L.F., 2012. Las tobas/travertinos del Barranco de Calabozo: un ejemplo
508 de construcción rápida de un edificio carbonático alimentado por una tubería de
509 regadío. *Geotemas* 13, 44-47.

510 Andrews, J.E., Rinding, R., Dennis, P.F., 1993. Stable isotopic composition of recent
511 fresh water cyanobacterial carbonates from the British Isles: local and regional
512 environmental controls. *Sedimentology* 40, 303-314.

513 Andrews, J.E., 2006. Palaeoclimatic records from stable isotopes in riverine tufas:
514 Synthesis and review. *Earth-Science Reviews* 75, 85-104.

515 Anzalone, E., Ferreri, V., Sprovieri, M., D'Argenio, B., 2007. Travertines as hydrologic
516 archives: The case of the Pontecagnano deposits (southern Italy). *Advances in*
517 *Water Resources* 30, 2159-2175.

518 Arenas, C., Cabrera, L., Ramos, E., 2007. Sedimentology of tufa facies and continental
519 microbialites from the Palaeogene of Mallorca Island (Spain). *Sedimentary Geology*
520 197, 1-27.

521 Aulinas, M., Gimeno, D., Fernández-Turiel, J.L., Font, L., Pérez-Torrado, F.J.,
522 Rodríguez-González, A., Nowell, G.M., 2010. Small-scale mantle heterogeneity on
523 the source of the Gran Canaria (Canary Islands) Pliocene-Quaternary magmas.
524 *Lithos* 119, 377-392.

525 Bottinga, Y., 1968. Calculation of fractionation factors for carbon and oxygen isotopic
526 exchange in the system calcite-carbon dioxide-water. *J. Phys. Chem.* 72, 800-808.

527 Buczynski, C., Chafetz, H.S., 1991. Habit of bacterially induced precipitates of calcium-
528 carbonate and the influence of medium viscosity on mineralogy. *Journal of*
529 *Sedimentary Petrology* 61, 226-233.

530 Calvet, F., 1982. Constructive micrite envelope developed in vadose continental
531 environment in pleistocene eolianites of Mallorca (Spain), *Acta Geológica*
532 *Hispánica*, pp. 169-178.

533 Capezzuoli, E., Gandin, A., Pedley., M., 2014. Decoding tufa and travertine (fresh
534 water carbonates) in the sedimentary record: The state of the art. *Sedimentology*
535 61, 1-21.

536 Carracedo, J.C., Day. S., Guillou, H., Rodríguez-Badiola, E., Canas, J.A., Pérez-
537 Torrado, F.J., 1998. Hotspot volcanism close to a passive continental margin: the
538 Canary Islands. *Geological Magazine* 135, 591-604.

539 Carracedo, J.C., Pérez-Torrado, F.J., Ancochea, E., Meco, J., Hernán, F., Cubas, C.R.,
540 Casillas, R., Rodríguez-Badiola, E., 2002. Cenozoic volcanism II: the Canary
541 Islands. In: Gibbons, F.A.W., Moreno, T. (eds.), *The Geology of Spain: Geological*
542 *Society*, London, pp. 438-472.

543 Castanier, S., Maurin, A., Perthuisot, J.P., 1989. Experimental bacterial production of
544 spheroidal, fibro-radial carbonate bodies - Discussions about the definition of ooids.
545 *Bulletin De La Societe Geologique De France* 5, 589-595.

546 Chacón, E., Berrendero, E., García-Pichel, F., 2006. Biogeological signatures of
547 microboring cyanobacterial communities in marine carbonates from Cabo Rojo,
548 Puerto Rico. *Sedimentary Geology* 185, 215-228.

549 Chafetz, H.S., Lawrence, J.R., 1994. Stable Isotopic Variability within Modern
550 Travertines. *Geographie Physique Et Quaternaire* 48, 257-273.

551 Custodio, E., Hoppe, J., Hoyos-Limón, A., Jiménez, J., Plata, A., Udluft, P., 1987. IV
552 Simposio de hidrogeología. *Asociación Española de Hidrogeología Subterránea*.
553 *Palma de Mallorca, Spain*, pp. 162-180.

554 D'Alessandro, W., Glammanco, S., Bellomo, S., Parello, F., 2007. Geochemistry and
555 mineralogy of travertine deposits of the SW flank of Mt. Etna (Italy): Relationships
556 with past volcanic and degassing activity. *Journal of Volcanology and Geothermal*
557 *Research* 165, 64-70.

558 Decho, A.W., Visscher, P.T., Reid, R.P., 2005. Production and cycling of natural
559 microbial exopolymers (EPS) within a marine stromatolite. *Palaeogeography*
560 *Palaeoclimatology Palaeoecology* 219, 71-86.

561 Demény, A., Kele, S., Siklósy, Z., 2010. Empirical equations for the temperature
562 dependence of calcite-water oxygen isotope fractionation from 10 to 70°C. *Rapid*
563 *Communications in Mass Spectrometry* 24 (24), 3521-3526.

564 Dietzel, M., Tang, J., Leis, A., Köhler, S.J., 2009. Oxygen isotopic fractionation during
565 inorganic calcite precipitation – Effects of temperature, precipitation rate and pH.
566 *Chemical Geology* 268, 107-115.

567 Dupraz, C., Visscher, P.T., 2005. Microbial lithification in marine stromatolites and
568 hypersaline mats. *Trends in Microbiology* 13, 429-438.

569 Dupraz, C., Visscher, P.T., Baumgartner, L.K., Reid, R.P., 2004. Microbe-mineral
570 interactions: early carbonate precipitation in a hypersaline lake (Eleuthera Island,
571 Bahamas). *Sedimentology* 51, 745-765.

572 Ford, T.D., Pedley, H.M., 1996. A review of tufa and travertine deposits of the world.
573 *Earth-Science Reviews* 41, 117-175.

574 Freytet, P., Verrecchia, E.P., 1999. Calcitic radial palisadic fabric in freshwater
575 stromatolites: diagenetic and recrystallized feature or physicochemical sinter crust?
576 *Sedimentary Geology* 126, 97-102.

577 Fouke, B.W., 2011. Hot-spring Systems Geobiology: abiotic and biotic influences on
578 travertine formation at Mammoth Hot Springs, Yellowstone National Park, USA.
579 *Sedimentology* 58, 170-219.

580 Gandin, A., Capezzuoli, E., 2008. Travertine versus Calcareous tufa: distinctive
581 petrologic features and related stable isotopes signature. *Il Quaternario, Italian*
582 *Journal of Quaternary Science* 21, 125-136.

583 Gandin, A., Capezzuoli, E., 2014. Travertine: Distinctive depositional fabrics of
584 carbonates from thermal spring systems. *Sedimentology* 61, 264-290.

585 García-del-Cura, M.A., Sanz-Montero, M.E., De-los-Ríos, M.A., Ascaso, C., 2014.
586 Microbial dolomite in fresh water carbonate deposits. *Sedimentology* 61, 41-55.

587 Garralda-Iribarren, M., 1952. Aportaciones al estudio de las aguas de Los Berrazales
588 de Agaete (Gran Canaria). Talleres tipográficos Peñate. Las Palmas de Gran
589 Canaria, Spain.

590 Gasparini, A., Custodio, E., Fontes, J.C., Jiménez, J., Nuñez, J.A., 1990. Exemple
591 d'étude géochimique et isotopique et circulations aquifères en terrain volcanique
592 sous climat semi-aride (Amurga, Gran Canaria, Iles Canaries). *Journal of*
593 *Hydrology* 114, 61-91.

594 Gautret, P., Camoin, G., Golubic, S., Sprachta, S., 2004. Biochemical control of
595 calcium carbonate precipitation in modern lagoonal microbialites, Tikehau atoll,
596 French Polynesia. *Journal of Sedimentary Research* 74, 462-478.

597 Goldsmith, J.R., Graf, D.L., Heard, H.C., 1961. Lattice constants of the calcium-
598 magnesium carbonates. *American Mineralogist* 46, 453-457.

599 Golubic, S., Radtke, G., Le Campion-Alsumard, T., 2005. Endolithic fungi in marine
600 ecosystems. *Trends in Microbiology* 13, 229-235.

601 Gonfiantini, R., Gallo, G., Payne, B.R., Taylor, C.B., 1976. Environmental isotopes and
602 hydrochemistry in groundwater of Gran Canaria. In: IAEA Staff (Eds.), *Interpretation*
603 *of Environmental Isotope and Hydrochemical Data in Groundwater Hydrology*.
604 IAEA, Vienna, pp. 159-170.

605 Gradziński, M., 2010. Factors controlling growth of modern tufa: results of a field
606 experiment. Geological Society, London, *Special Publications* 336, 143-191.

607 Gradziński, M., Hercman, H., Jaśkiewicz, M., Szczurek, S., 2013. Holocene tufa in the
608 Slovak Karst: facies, sedimentary environments and depositional history.
609 Geological Quarterly 57, 769-788.

610 Gradziński, M., Wróblewski, W., Duliński, M., Hercman, H., 2014. Earthquake-affected
611 development of a travertine ridge. Sedimentology 61, 238-263.

612 Guillou, H., Pérez-Torrado, F.J., Hansen-Machin, A.R., Carracedo, J.C., Gimeno, D.,
613 2004. The Plio-Quaternary volcanic evolution of Gran Canaria based on new K-Ar
614 ages and magneto stratigraphy. Journal of Volcanology and Geothermal Research
615 135, 221-246.

616 Guo, L., Riding, R., 1992. Aragonite laminae in hot water travertine crusts, Rapolano
617 Terme, Italy. Sedimentology 39, 1067-1079.

618 Guo, L., Chafetz, H.S., 2014. Trends in $\delta^{18}\text{O}$ and $\delta^{13}\text{C}$ values in lacustrine tufa
619 mounds: Palaeohydrology of Searles Lake, California. Sedimentology 61, 221-237.

620 Halas, S., Wolacewicz, W., 1982. The experimental study of oxygen isotope exchange
621 reaction between dissolved bicarbonate and water. Journal of Chemical Physics
622 76, 5470-5472.

623 Hancock, P.L., Chalmers, R.M.L., Altunel, E., Çakir, Z., 1999. Travitronics: using
624 travertines in active fault studies. Journal of Structural Geology 21, 903-916.

625 Hoefs, J., 1997. Stable isotope geochemistry. Springer Verlag, Berlin.

626 Holik, J.S., Rabinowitz, P.D., Austin, J.A., 1991. Effects of Canary hotspot volcanism
627 on structure of oceanic crust off Morocco. Journal of Geophysical Research: Solid
628 Earth 96, 12039-12067.

629 Janssen, A., Swennen, R., Podoor, N., Keppens, E., 1999. Biological and diagenetic
630 influence in Recent and fossil tufa deposits from Belgium. Sedimentary Geology
631 126, 75-95.

632 Jones, B., Kahle, C.F., 1986. Dendritic Calcite Crystals Formed by Calcification of Algal
633 Filaments in a Vadose Environment. Journal of Sedimentary Petrology 56, 217-
634 227.

635 Jones, B., Kahle, C.F., 1993. Morphology, relationship, and origin of fiber and dendrite
636 calcite crystals. *Journal of Sedimentary Petrology* 63, 1018-1031.

637 Jones, B., Kahle, C.F., 1995. Origin of endogenetic micrite in karst terrains: a case
638 study from the Cayman Islands. *Journal of Sedimentary Research* 65, 283-293.

639 Jones, B., Renaut, R.W., 1996. Morphology and growth of aragonite crystals in hot-
640 spring travertines at Lake Bogoria, Kenya Rift Valley. *Sedimentology* 43, 323-340.

641 Jones, B., Renaut, R.W., 2008. Cyclic development of large, complex, calcite dendrite
642 crystals in the Clinton travertine, Interior British Columbia, Canada. *Sedimentary*
643 *Geology* 203, 17-35.

644 Jones, B., Renaut, R.W., 2010. Calcareous Spring Deposits in Continental Settings. In:
645 Alonso-Zarza, A.M., Tarnner, L.H. (Eds), *Carbonates in Continental settings.*
646 *Facies, Environments and Processes.* Elsevier, Amsterdam, pp. 177-224.

647 Jones, B., Renaut, R.W., Rosen, M.R., 2000. Trigonal dendritic calcite crystals forming
648 from hot spring waters at Waikite, North Island, New Zealand. *Journal of*
649 *Sedimentary Research* 70, 586-603.

650 Jones, B., Renaut, R.W., Owen, R.B., Torfason, H., 2005. Growth patterns and
651 implications of complex dendrites in calcite travertines from Lýsuhóll, Snæfellsnes,
652 Iceland. *Sedimentology* 52, 1277-1301.

653 Kele, S., Demény, A., Siklósy, Z., Németh, T., Mária, T., Kovács, M.B., 2008. Chemical
654 and stable isotope composition of recent hot-water travertines and associated
655 thermal waters, from Egerszalók, Hungary: depositional facies and non-equilibrium
656 fractionations. *Sedimentary Geology* 211, 53-72.

657 Kele, S., Özkul, M., Fórizs, I., Gökgöz, A., Baykara, M.O., Alçiçek, M.C., Németh, T.,
658 2011. Stable isotope geochemical study of Pamukkale travertines: New evidences
659 of low-temperature non-equilibrium calcite-water fractionation. *Sedimentary*
660 *Geology* 238, 191-212.

661 Keppel, M.N., Post, V.E.A., Love, A.J., Clarke, J.D.A., Werner, A.D., 2012. Influences
662 on the carbonate hydrochemistry of mound spring environments, Lake Eyre South
663 region, South Australia. *Chemical Geology* 296-297, 50-65.

664 Kim, S.T., O'Neil, J.R., 1997. Equilibrium and nonequilibrium oxygen isotope effects in
665 synthetic carbonates. *Geochímica et Cosmochimica Acta* 61, 3461-3475.

666 Kobluk, D.R., Risk, M.J., 1977. Calcification of exposed filaments of endolithic algae,
667 micrite envelope formation and sediment production. *Journal of Sedimentary*
668 *Research* 47, 517-528.

669 Krumbein, W.E., Cohen, Y., Shilo, M., 1977. Solar lake (Sinai). 4. Stromatolitic
670 cyanobacterial mats, *Limnology and Oceanography* 22, pp. 635-655.

671 Martín-García, R., Alonso-Zarza, A.M., Martín-Pérez, A., 2009. Loss of primary texture
672 and geochemical signatures in speleothems due to diagenesis: Evidences from
673 Castanar Cave, Spain. *Sedimentary Geology* 221, 141-149.

674 McCrea, J.M., 1950. On the Isotopic Chemistry of Carbonates and a Paleotemperature
675 Scale. *The Journal of Chemical Physics* 18, pp. 849-857.

676 Minissale, 2004. Origin, transport and discharge of CO₂ in central Italy. *Earth-Science*
677 *Reviews* 66, 89-141.

678 Mook, W.G., Bommerson, J.C., Staverman, W.H., 1974. Carbon isotope fractionation
679 between dissolved bicarbonate and gaseous carbon dioxide. *Earth and Planetary*
680 *Science Letters* 22 (2), 169-176.

681 Nishikawa, O., Furuhashi, K., Masashi, M., Takeyuki, O., Shiraishi, T., Shen, C., 2012.
682 Radiocarbon dating of residual organic matter in travertine formed along the
683 Yumoto Fault in Oga Peninsula, northeast Japan: Implications for long-term hot
684 spring activity under the influence of earthquakes. *Sedimentary Geology* 243-244,
685 181-190.

686 Okumura, T., Takashima, C., Shiraishi, F., Akmaluddin, Kano, A., 2012. Textural
687 transition in an aragonite travertine formed under various flow conditions at
688 Pancuran Pitu, Central Java, Indonesia. *Sedimentary Geology* 265, 195-209.

689 Okumura, T., Takashima, C., Kano, A., 2013a. Textures and processes of laminated
690 travertines formed by unicellular cyanobacteria in Myoken hot spring, southwestern
691 Japan. *Island Arc* 22, 410-426.

692 Okumura, T., Takashima, C., Shiraishi, F., Nishida, S., Kano, A., 2013b. Processes
693 Forming Daily Lamination in a Microbe-Rich Travertine Under Low Flow Condition
694 at the Nagano-yu Hot Spring, Southwestern Japan. *Geomicrobiology Journal* 30,
695 910-927.

696 Özkul, M., 2005. Travertine deposits of Denizli Extensional Basin in Western Turkey: a
697 general review. *Proceedings of 1st International Symposium on TRAVERTINE.*
698 Pamukkale University, Denizli, Turkey, pp. 18-24.

699 Özkul, M., Kele, S., Gökgöz, A., Shen, C.C., Jones, B., Baykara, M.O., Főrizs I.,
700 Németh, T., Chang, Y.W., Alçiçek, M.C., 2013. Comparison of the Quaternary
701 travertines sites in the Denizli extensional basin based on their depositional and
702 geochemical data. *Sedimentary Geology* 294, 179-204.

703 Özkul, M., Gökgöz, A., Kele, S., Baykara, M.O., Shen, C.C., Chang, Y.W., Kaya, A.,
704 Hançer, M., Aratman, C., Akin, T., Örü, Z., 2014. Sedimentological and
705 geochemical characteristics of a fluvial travertine: A case from the eastern
706 Mediterranean region. *Sedimentology* 61, 291-318.

707 Panichi, C., Tongiorgi, E., 1976. Carbon isotopic composition of CO₂ from springs,
708 fumaroles, mofettes and travertines of central and southern Italy: a preliminary
709 prospection method of geothermal area. *Proc. 2nd UN Symposium on the Develop
710 and Use of Geothermal Energy.* San Francisco, U.S.A, pp. 815-825.

711 Pedley, M., 1992. Freshwater (phytoherm) reefs: the role of biofilms and their bearing
712 on marine reef cementation. *Sedimentary Geology* 79, 255-274.

713 Pentecost, A., 1995. The quaternary travertine deposits of Europe and Asia Minor.
714 *Quaternary Science Reviews* 14, 1005-1028.

715 Pentecost, A., 2005. *Travertine.* 445 pp. Springer, Berlin.

716 Perez-Torrado, F.J., Carracedo, J.C., Mangas, J., 1995. Geochronology and
717 stratigraphy of the Rogue Nublo Cycle, Gran-Canaria, Canary Islands. *Journal of*
718 *the Geological Society* 152, 807-818.

719 Perri, E., Manzo, E., Tucker, M.E., 2012. Multi-scale study of the role of the biofilm in
720 the formation of minerals and fabrics in calcareous tufa. *Sedimentary Geology* 263,
721 16-29.

722 Pola M., Gandin, A., Tuccimei, P., Soligo, M., Deiana, R., Fabbri, P., Zampieri, D.,
723 2014. A multidisciplinary approach to understanding carbonate deposition under
724 tectonically controlled hydrothermal circulation: A case study from a recent
725 travertine mound in the Eugenean hydrothermal system, northern Italy.
726 *Sedimentology* 61, 172-199.

727 Radtke, G., Golubic, S., 2011. Microbial euendolithic assemblages and microborings in
728 intertidal and shallow marine habitats. *Advances in Stromatolite Geobiology* 131,
729 233-263.

730 Renaut, R.W., Jones, B., 1997. Controls on aragonite and calcite precipitation in hot
731 spring travertines at Chemurkeu, Lake Bogoria, Kenya. *Canadian Journal of Earth*
732 *Sciences* 34, 801-818.

733 Riding, R., 2008. Abiogenic, microbial and hybrid authigenic carbonate crusts:
734 components of Precambrian stromatolites. *Geologia Croatica* 61, 73-103.

735 Ries, J.B., Anderson, M.A., Hill, R.T., 2008. Seawater Mg/Ca controls polymorph
736 mineralogy of microbial CaCO₃: A potential proxy for calcite-aragonite seas in
737 Precambrian time. *Geobiology* 6, 106-119.

738 Rodríguez-Berriguete, A., Alonso-Zarza, A.M., Cabrera, M.C., Rodríguez-González, A.,
739 2012. The Azuaje travertine: an example of aragonite deposition in a recent
740 volcanic setting, N Gran Canaria Island, Spain. *Sedimentary Geology* 277-278, 61-
741 71.

742 Rodríguez-González, A., Fernández-Turiel, J.L., Pérez-Torrado, F.J., Hansen, A.,
743 Aulinas, M., Carracedo, J.C., Gimeno, D., Guillou, H., Paris, R., Paterne, M., 2009.

744 The Holocene volcanic history of Gran Canaria Island: implications for volcanic
745 hazards. *Journal of Quaternary Science* 24, 697-709.

746 Rodríguez-González, A., Fernández-Turiel, J.L., Pérez-Torrado, F.J., Paris, R.,
747 Gimeno, D., Carracedo, J.C., Aulinas, M., 2012. Factors controlling the morphology
748 of monogenetic basaltic volcanoes: the Holocene volcanism of Gran Canaria
749 (Canary Islands, Spain). *Geomorphology* 136, 31-44.

750 Scholle, P.A., Ulmer-Scholle, D.S., 2003. A color guide to the petrography of carbonate
751 rocks: grains, textures, porosity, diagenesis. AAPG Memoir 77. 474 pp. Tulsa,
752 Oklahoma.

753 Sun, H., Liu, Z., Yan., H., 2014. Oxygen isotope fractionation in travertine-depositing
754 pools at Baishuitai, Yunnan, SW China: Effects of deposition rates. *Geochimica et*
755 *Cosmochimica Acta*, In press.

756 Talbot, M.R., 1990. A review of the palaeohydrological interpretation of carbon and
757 oxygen isotopic ratios in primary lacustrine carbonates. *Chemical Geology: Isotope*
758 *Geoscience section* 80, 261-279.

759 Terra, G.J.S., Spadini, A.R., Franca, A.B., Sombra, C.L., 2010. Carbonate rock
760 classification applied to Brazilian sedimentary basins. *Boletim Geociencias*
761 *Petrobras* 18. Rio de Janeiro, Brazil, pp. 9-29.

762 Tucker, M.E., 1988. *Techniques in sedimentology*. 394 pp. Oxford England, Boston.

763 Turner, E.C., Jones, B., 2005. Microscopic calcite dendrites in cold-water tufa:
764 implications for nucleation of micrite and cement. *Sedimentology* 52, 1043-1066.

765 Valero-Garcés, B., Arenas, C., Delgado-Huertas, A., 2001. Depositional environments
766 of Quaternary lacustrine travertines and stromatolites from high-altitude Andean
767 lakes, northwestern Argentina. *Canadian Journal of Earth Sciences* 38, 1263-1283.

768 Viles, H., Pentecost, A., 2008. Tufa and Travertine. In: Nash, D.J., McLaren, S.J.
769 (Eds.), *Geochemical Sediments and Landscapes*. Blackwell Publishing Ltd.,
770 Oxford, pp. 173-199.

771

772

773 **Figure captions**

774

775 **Fig. 1.** (A) Location of the Berrazales area, in the north-west of Gran Canaria Island.
776 (B) Situation of the Berrazales Carbonate Deposit (BCD) between volcanic materials in
777 the Barranco Los Ríos.

778

779 **Fig. 2.** (A) Photograph of the main part of Berrazales deposit. (B) Sketch from
780 Photograph A, showing the dominance of cascade facies and location of the samples.
781 Two molds of trunks can be observed (red arrows). The carbonate deposits overlie the
782 volcanic lava.

783

784 **Fig. 3.** Photographs of *Fibrous dense macrocrystalline* facies. (A) Fibrous feather or
785 dendrite crystals separated by dark micritic laminae. (B) Microbial filaments (arrows)
786 encased within feather dendrite crystals. (C) Tops of crystalline feathers are micritized
787 (arrows). (D) Detailed view of the red rectangle of C, showing microbial filaments
788 penetrating large crystals and generating circular microborings (arrow). (E) SEM image
789 of circular microbial filament microborings. (F) SEM image showing parallel porosity
790 created by penetration of a network of microbial filaments.

791

792 **Fig. 4.** (A) *Framestone* facies composed of parallel plant molds coated with calcite. (B)
793 Plant mold surrounded by coarse calcite crystals. (C) SEM image showing parallel
794 structure of plants molds. (D) *Micrite-coarse crystalline banded* facies with reddish-
795 translucent (1) and dark-micritic (2) laminae. Arrows show V-shaped morphologies,
796 located between the edges of palisade crystals.

797

798 **Fig.5.** Photographs of *Micrite/microsparitic* facies. (A) Crystalline microsparitic
799 aggregates growing from organic filaments within a micritic mass. (B) Microsparitic
800 band composed of crystalline fans in a porous micritic mass. (C) Dendrolitic fabric
801 composed of calcified cyanobacterial filaments. (D) SEM image of a calcified filament
802 in transverse view. Arrow indicates the central hole left by dissolved filament. (E)
803 Exopolymeric substances (EPS) (arrows) intercalated within calcite crystals and
804 cyanobacterial filaments (f). (F) Detail of EPS (arrows).

805

806 **Fig. 6.** (A) Calcite crystals penetrated by a network of microbes. (B) Fibrous feather
807 calcite crystals intercalated with altered micritic masses. (C) Detail of calcite crystals
808 penetrated and altered by thin microbial filaments (arrows).

809

810 **Fig. 7.** Stable carbon and oxygen isotope composition of Berrazales carbonate deposit
811 samples according to: (A) facies and (B) Mg content.

812

813 **Fig. 8.** Growth phases of fibrous branching feather or dendrite morphologies. (A)
814 Microbial filament. (B) Sparite nucleating on biogenic support. (C) Abiogenic growth of
815 fibrous calcite crystals. (D) Perforation and micritization of fibrous calcite by microbes
816 (cyanobacteria or fungi).

817

818 **Fig. 9.** Stable isotope composition of some travertines and tufas from the world
819 including the data from this study.

820

821 **Table 1.** Berrazales carbonate deposit samples: type of facies; mineralogy; principal
822 calcite peak with the respective content of MgCO₃; and stable isotope composition.

823

824 **Table 2.** Calculations of: $\delta^{18}\text{O}_{\text{calcite}}$ (‰, VSMOW); $\delta^{18}\text{O}_{\text{water}}$ (‰, VSMOW); $\Delta\text{HCO}_3\text{--H}_2\text{O}$;
825 and Temperature under disequilibrium and equilibrium conditions. (A) Calculated with
826 $\delta^{18}\text{O}_{\text{water}} = -3.33\text{‰}$ VSMOW. (B) Calculated with $\delta^{18}\text{O}_{\text{water}} = -5.50\text{‰}$ VSMOW.

827

828 **Table 3.** Calculation of the original $\delta^{13}\text{C}_{\text{CO}_2}$ from calculated temperatures of the
829 crystalline crust (BER-11) (see temperature in disequilibrium from Table 2A, B).
830 $\delta^{13}\text{C}_{\text{CO}_2}$ is calculated with equations of Mook et al. (1974), Panichi and Tongiorgi
831 (1976), and Bottinga (1968).

Figure
[Click here to download high resolution image](#)

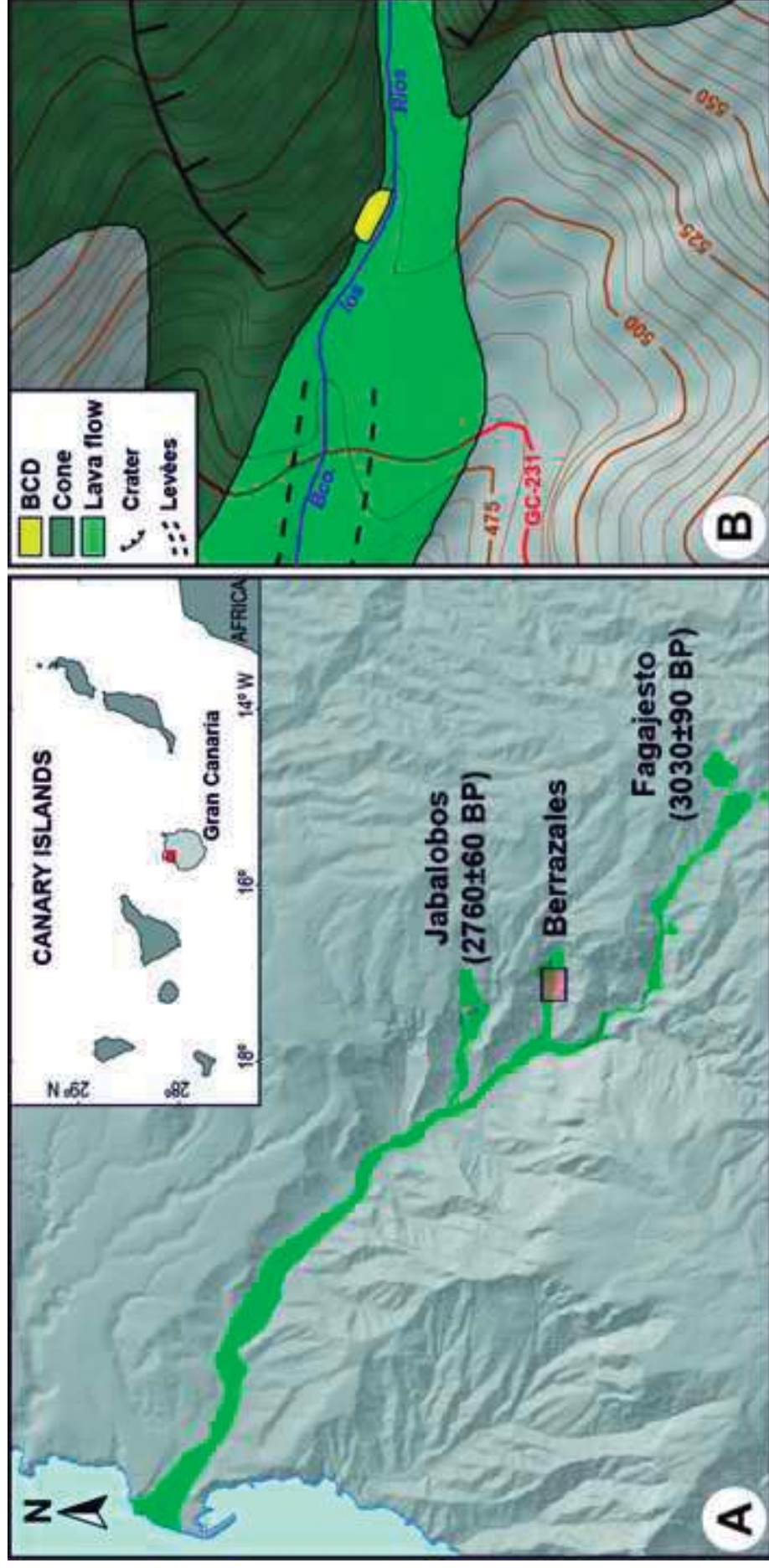


Figure
[Click here to download high resolution image](#)

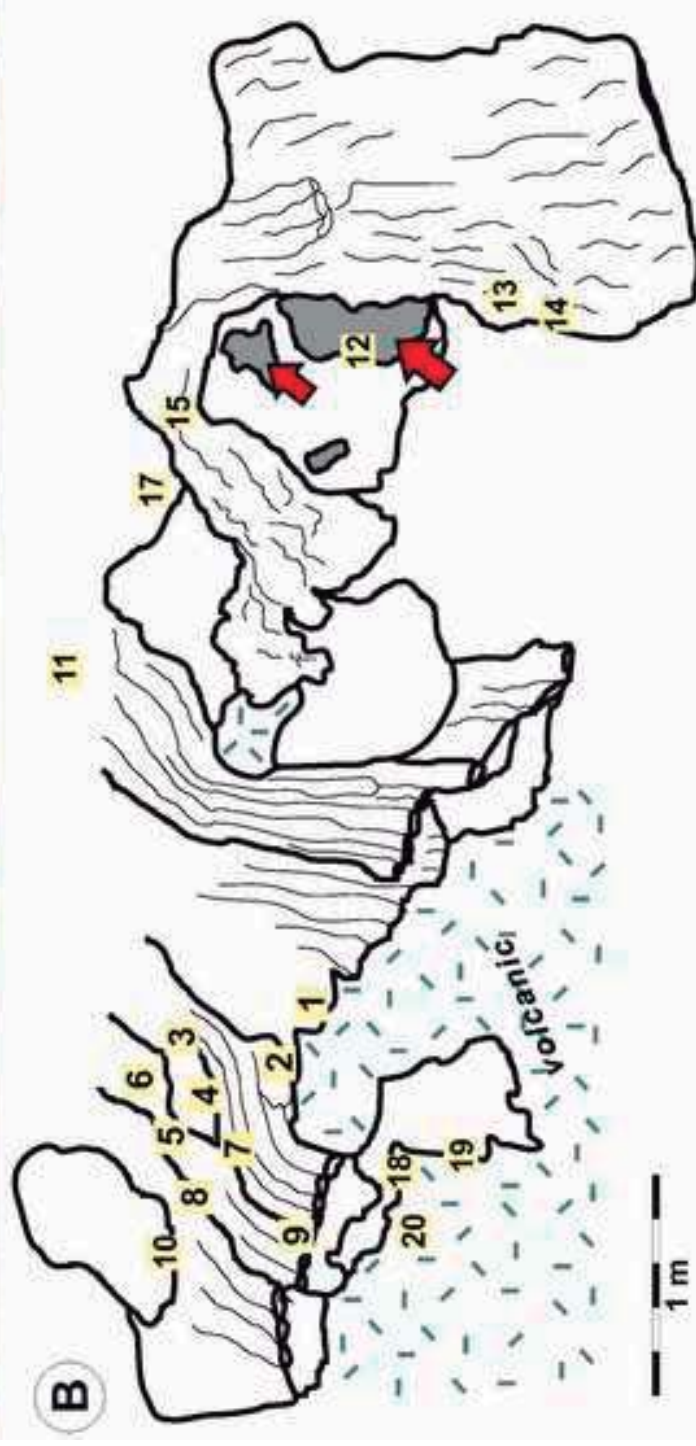


Figure
[Click here to download high resolution image](#)

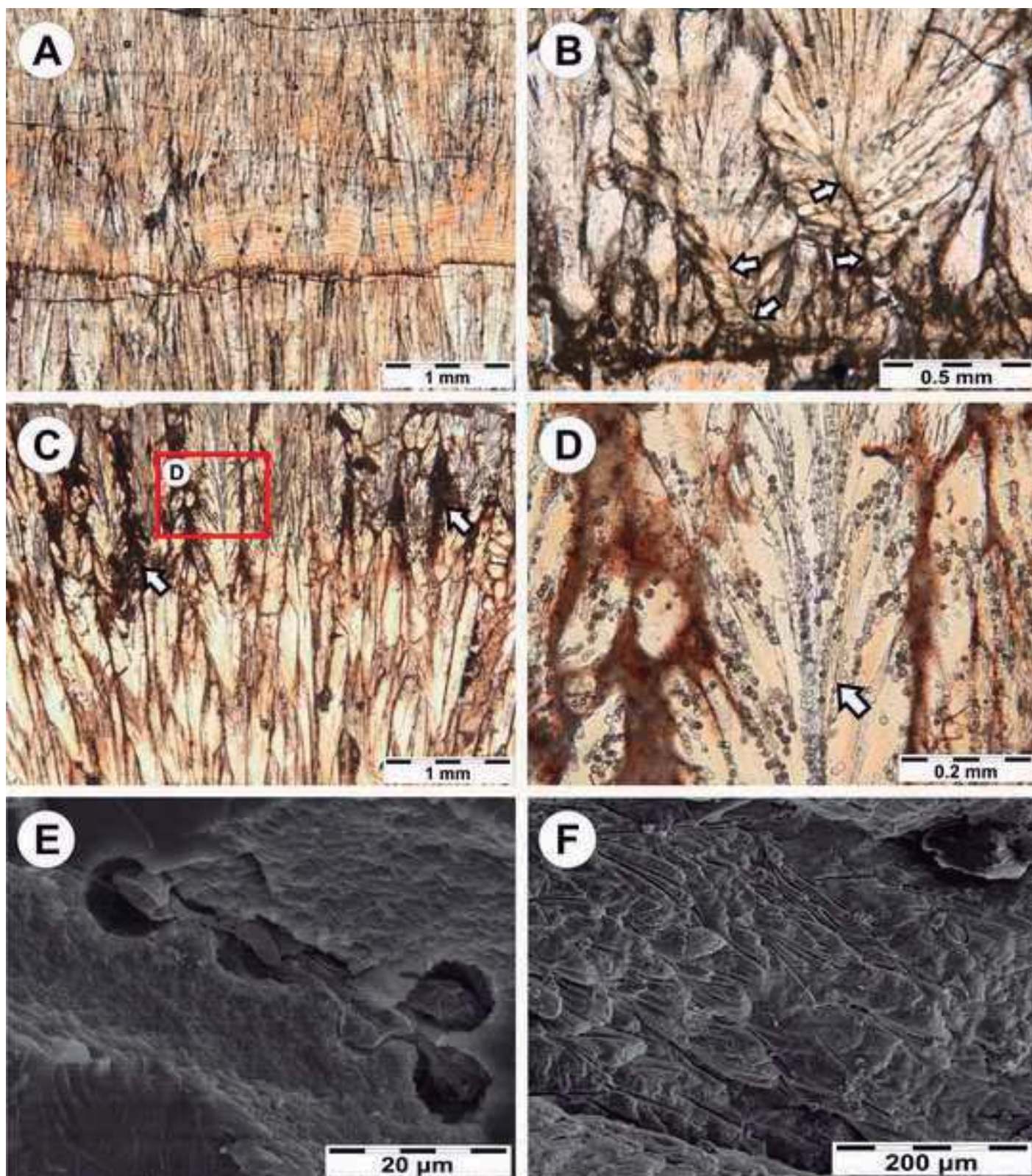


Figure
[Click here to download high resolution image](#)

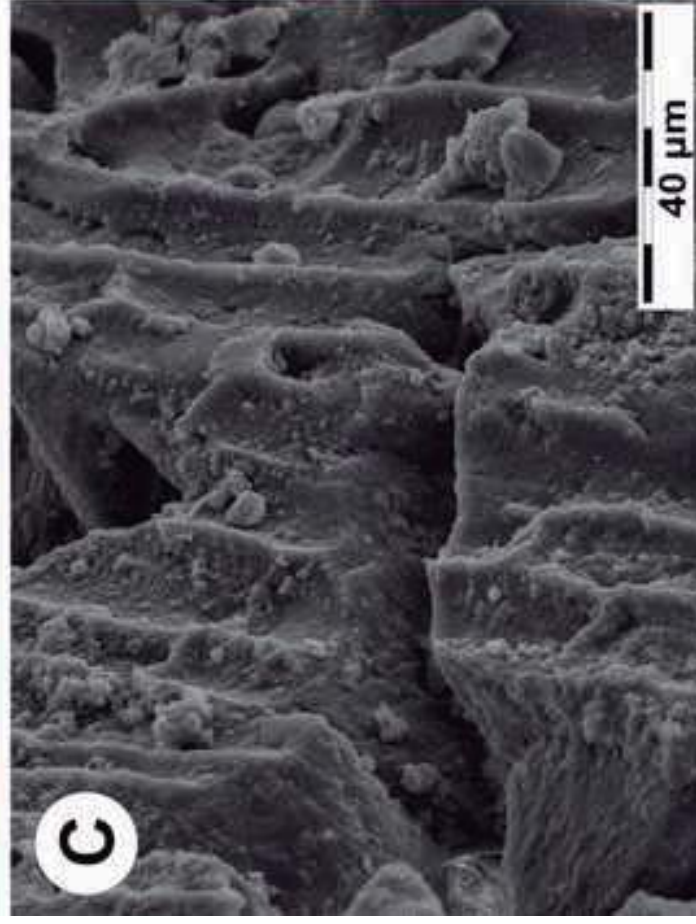


Figure
[Click here to download high resolution image](#)

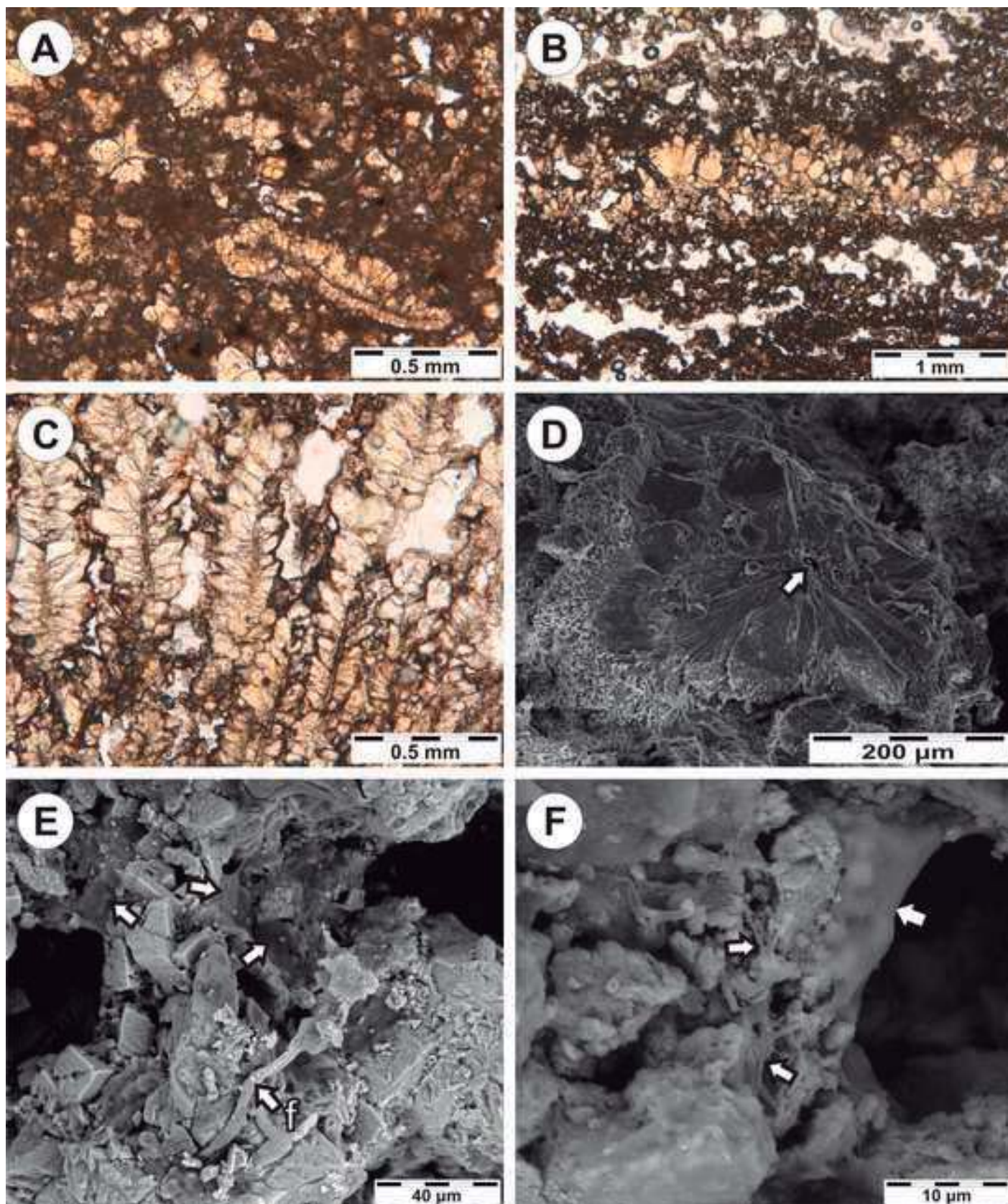


Figure
[Click here to download high resolution image](#)

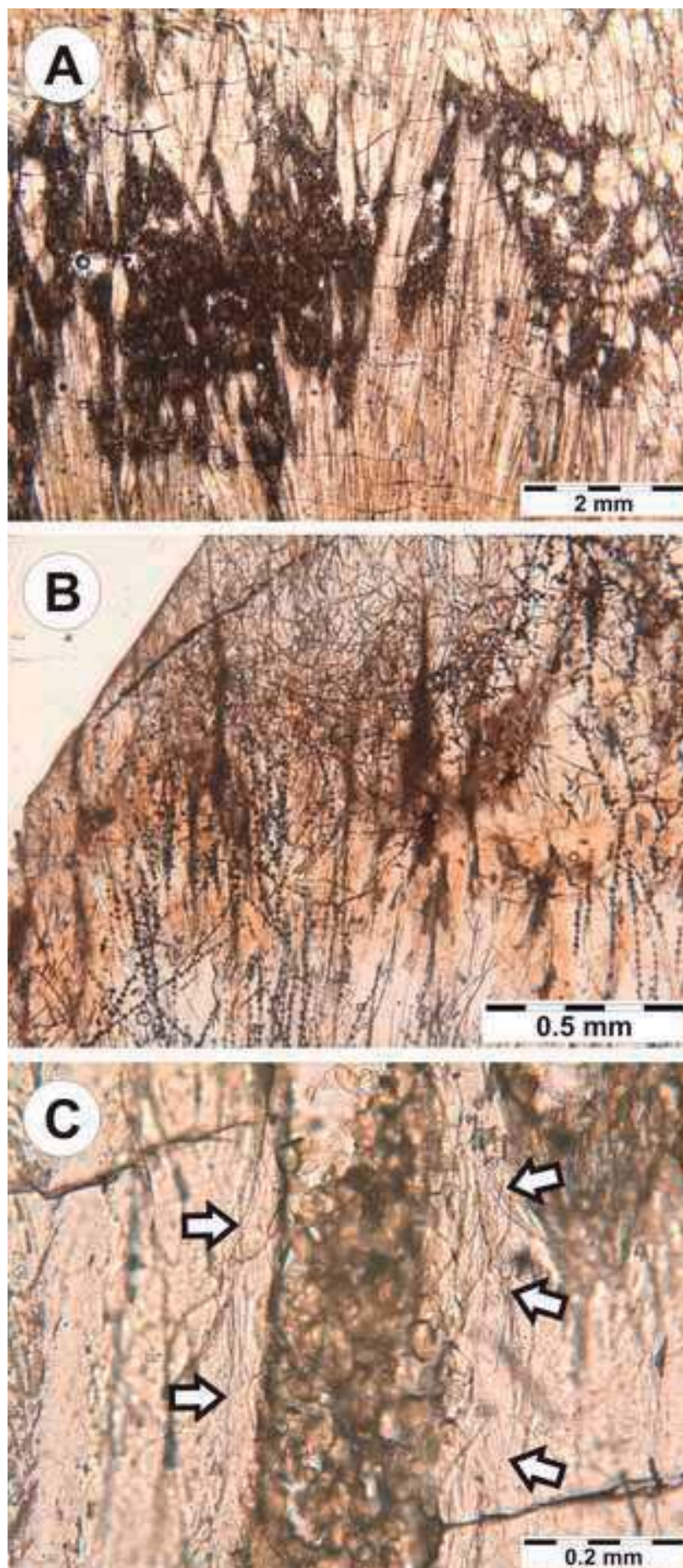


Figure
Click here to download high resolution image

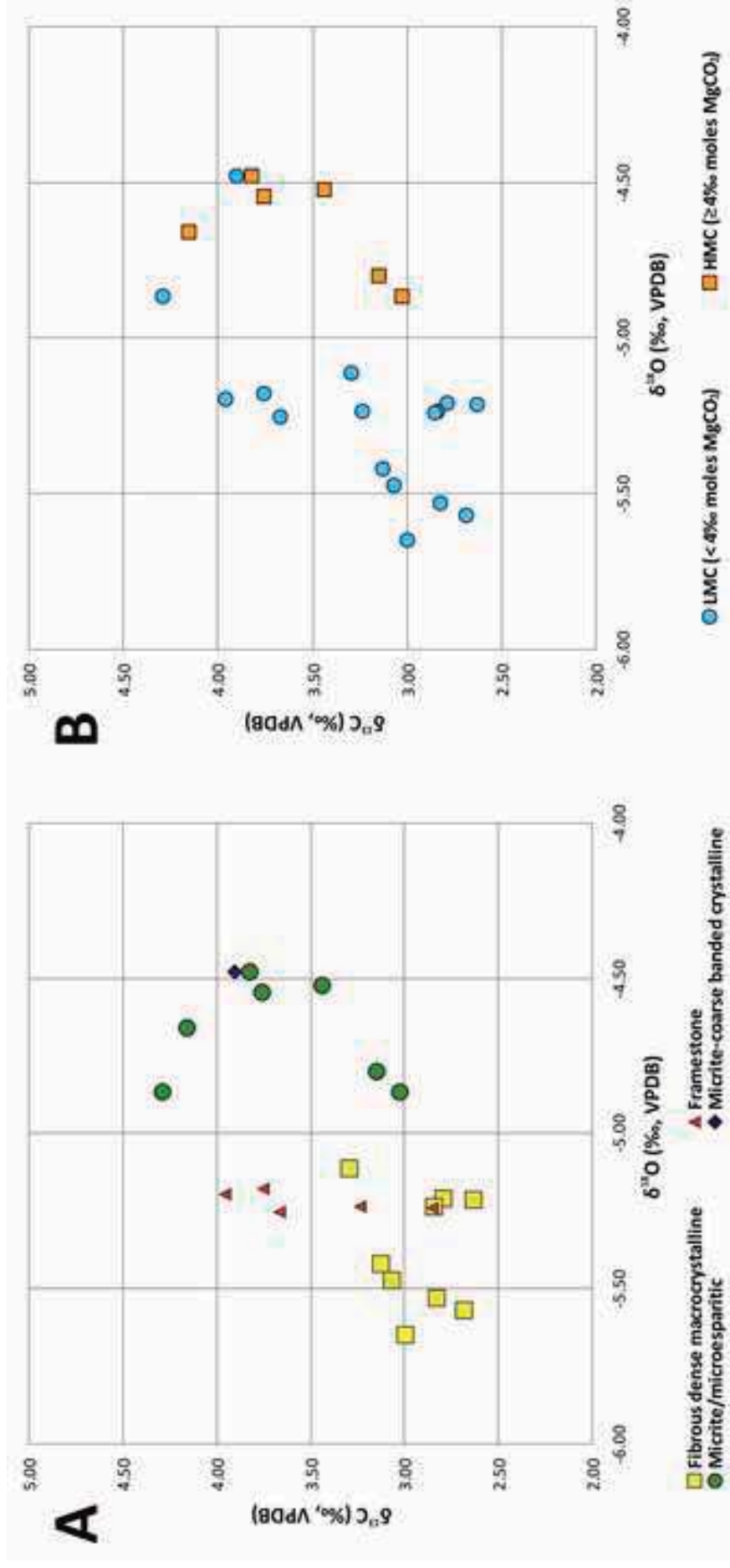
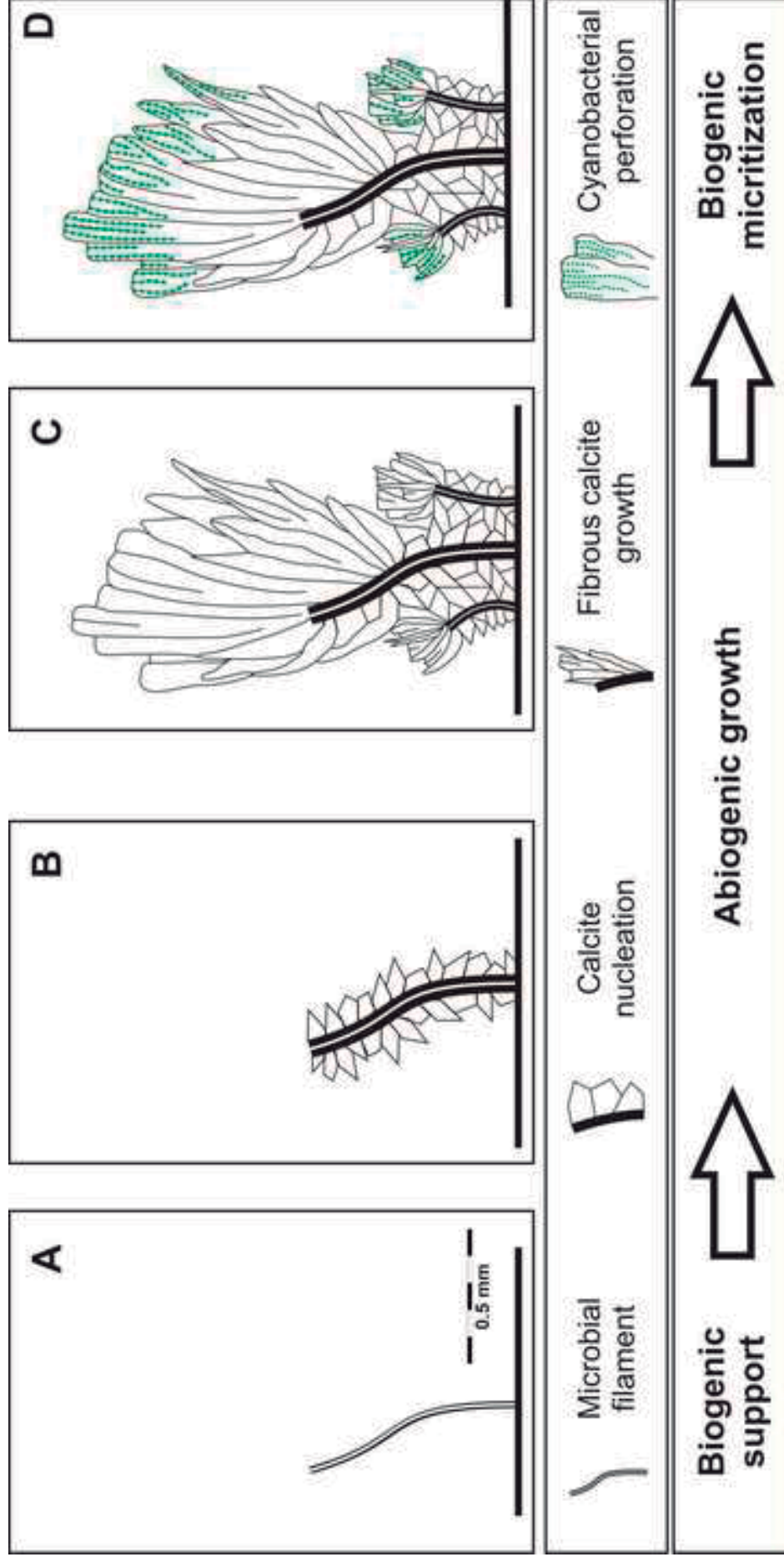
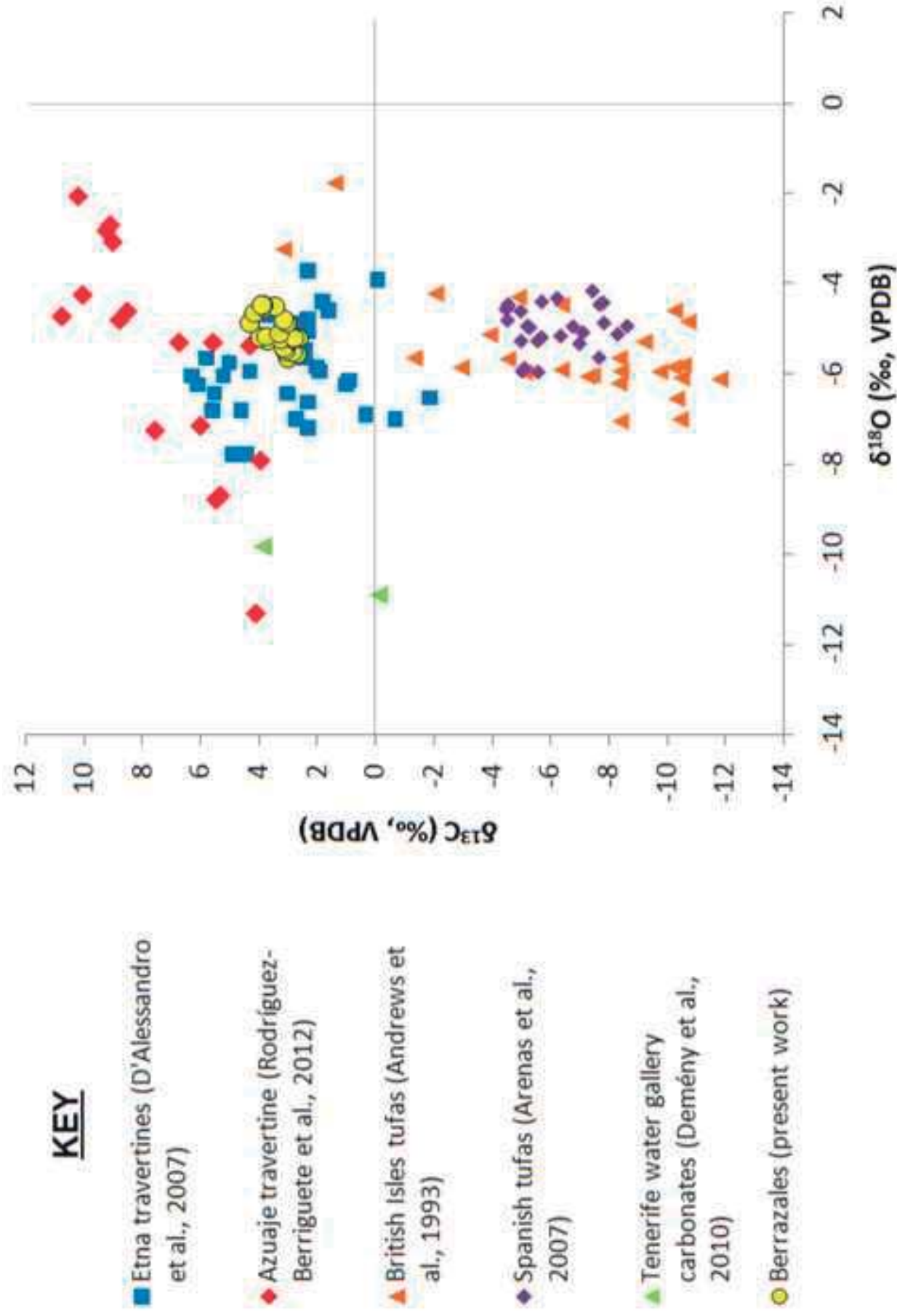


Figure
[Click here to download high resolution image](#)





Sample	Type of Facies	Mineralogy (Semi-quantitative)		Principal calcite peak (°2 θ)	% Moles MgCO ₃	$\delta^{13}\text{C}_{\text{calcite}}$ (‰, VPDB)	$\delta^{18}\text{O}_{\text{calcite}}$ (‰, VPDB)
		% Calcite	% Phyllosilicates				
BER-1	Framestone	100	*	29.16	0	3.67	-5.25
BER-2	Micrite-microsparitic	100	*	29.58	5	3.15	-4.80
BER-3	Fibrous dense macrocrystalline	100	*	29.46	2	2.83	-5.53
BER-3.1	Fibrous dense macrocrystalline	100	*	29.48	2	2.63	-5.21
BER-4	Fibrous dense macrocrystalline	100	*	29.48	2	2.69	-5.57
BER-5	Fibrous dense macrocrystalline	100	*	29.46	2	3.00	-5.65
BER-6	Framestone	100	*	29.46	2	3.24	-5.23
BER-7	Fibrous dense macrocrystalline	100	*	29.48	2	3.07	-5.47
BER-8	Micrite-microsparitic	90	10	29.54	4	3.82	-4.48
BER-9	Fibrous dense macrocrystalline	100	*	29.48	2	3.30	-5.11
BER-10	Fibrous dense macrocrystalline	100	*	29.44	2	3.12	-5.42
BER-11	Fibrous dense macrocrystalline	100	*	29.45	2	2.79	-5.21
BER-11.1	Fibrous dense macrocrystalline	100	*	29.45	2	2.84	-5.24
BER-12	Micrite-microsparitic	90	10	29.5	3	4.29	-4.86
BER-13	Framestone	100	*	29.5	3	3.96	-5.20
BER-14	Framestone	100	*	29.48	2	3.75	-5.18
BER-15	Micrite-microsparitic	100	*	29.57	5	4.15	-4.66
BER-17	Micrite-microsparitic	100	*	29.54 - 29.77	4 - 11	3.76	-4.55
BER-18	Framestone	100	*	29.46	2	2.85	-5.24
BER-18.1	Micrite-microsparitic	100	*	29.54	4	3.03	-4.87
BER-19	Micrite-microsparitic	100	*	29.58	5	3.44	-4.52
BER-20	Micrite-coarse banded crystalline	100	*	29.31	0	3.90	-4.48

Asterisks (*) indicate that the proportion of phyllosilicates is below 5%

Table 2A

Sample	$\delta^{18}\text{O}_{\text{calcite}}$ (‰, VSMOW)	$\Delta\text{HCO}_3^- - \text{H}_2\text{O}$	T diseq.(°C) ⁽¹⁾	T eq.(°C) ⁽²⁾
BER-1	25.13	28.46	33.3	23.2
BER-2	25.59	28.92	31.1	20.9
BER-3	24.84	28.17	34.8	24.6
BER-3.1	25.17	28.50	33.1	23.0
BER-4	24.80	28.13	34.9	24.8
BER-5	24.72	28.05	35.4	25.2
BER-6	25.15	28.48	33.2	23.1
BER-7	24.90	28.23	34.5	24.3
BER-8	25.92	29.25	29.5	19.4
BER-9	25.27	28.60	32.6	22.5
BER-10	24.96	28.29	34.2	24.0
BER-11	25.17	28.50	33.1	23.0
BER-11.1	25.14	28.47	33.3	23.1
BER-12	25.53	28.86	31.4	21.2
BER-13	25.19	28.52	33.0	22.9
BER-14	25.20	28.53	33.0	22.8
BER-15	25.74	29.07	30.4	20.2
BER-17	25.85	29.18	29.8	19.7
BER-18	25.14	28.47	33.3	23.1
BER-18.1	25.53	28.86	31.4	21.2
BER-19	25.88	29.21	29.7	19.6
BER-20	25.92	29.25	29.5	19.3

⁽¹⁾ $10^3 \ln \alpha (\text{HCO}_3^- - \text{H}_2\text{O})_{\text{eq.}} \approx 10^3 \ln \alpha (\text{CaCO}_3 - \text{H}_2\text{O})_{\text{diseq.}} = 2.92 \times 10^6 / T^2 - 2.66$ (Halas and Wolacewicz, 1982)

⁽²⁾ $10^3 \ln \alpha (\text{CaCO}_3 - \text{H}_2\text{O}) = 18.03 \times 10^3 / T - 32.42$ (Kim and O'Neil, 1997)

Table 2B

$\delta^{18}\text{O}_{\text{calcite}}$ (‰, VSMOW)	$\Delta\text{HCO}_3^- - \text{H}_2\text{O}$	T diseq.(°C) ⁽¹⁾	T eq.(°C) ⁽²⁾
25.13	30.63	23.2	13.0
25.59	31.09	21.1	10.9
24.84	30.34	24.5	14.3
25.17	30.67	23.0	12.8
24.80	30.30	24.6	14.5
24.72	30.22	25.0	14.8
25.15	30.65	23.1	12.9
24.90	30.40	24.2	14.0
25.92	31.42	19.7	9.4
25.27	30.77	22.5	12.3
24.96	30.46	23.9	13.8
25.17	30.67	23.0	12.8
25.14	30.64	23.1	12.9
25.53	31.03	21.4	11.2
25.19	30.69	22.9	12.7
25.20	30.70	22.8	12.6
25.74	31.24	20.5	10.2
25.85	31.35	20.0	9.7
25.14	30.64	23.1	12.9
25.53	31.03	21.4	11.2
25.88	31.38	19.9	9.6
25.92	31.42	19.7	9.4

Table

[Click here to download Table: Table 3.xls](#)

Author	Equation	Temperature (°C)	$\delta^{13}\text{C}_{\text{CO}_2}$ (‰, VPDB)
Mook et al. (1974)	$10^3 \ln \alpha (\text{HCO}_3^- - \text{CO}_2(\text{g})) = 9.552 \times (10^3/T) - 24.1$	33	-4.31
		23	-5.38
Panichi and Tongiorgi (1976)	$\delta^{13}\text{C}_{\text{CO}_2(\text{g})} = 1.2 \times \delta^{13}\text{C}_c - 10.5$	independent	-7.15
Bottinga (1968)	$10^3 \ln \alpha_c = -2.4912 + (7.663 \times 10^3/T) - (2.9880 \times 10^6/T^2)$	33	-6.58
		23	-7.95